

## Emergence of Topologically Nontrivial Spin-Polarized States in a Segmented Linear Chain

Thang Pham,<sup>1,2,3,4,\*</sup> Sehoon Oh<sup>Ⓜ</sup>,<sup>1,2,\*</sup> Scott Stonemeyer,<sup>1,2,4,5</sup> Brian Shevitski,<sup>1,2</sup> Jeffrey D. Cain<sup>Ⓜ</sup>,<sup>1,2,4</sup>  
Chengyu Song<sup>Ⓜ</sup>,<sup>6</sup> Peter Ercius<sup>Ⓜ</sup>,<sup>6</sup> Marvin L. Cohen,<sup>1,2</sup> and Alex Zettl<sup>1,2,4,†</sup>

<sup>1</sup>Department of Physics, University of California at Berkeley, Berkeley, California 94720, USA

<sup>2</sup>Materials Sciences Division, Lawrence Berkeley National Laboratory, Berkeley, California 94720, USA

<sup>3</sup>Department of Materials Science and Engineering, University of California at Berkeley, Berkeley, California 94720, USA

<sup>4</sup>Kavli Energy NanoSciences Institute at the University of California at Berkeley, Berkeley, California 94720, USA

<sup>5</sup>Department of Chemistry, University of California at Berkeley, Berkeley, California 94720, USA

<sup>6</sup>National Center for Electron Microscopy, The Molecular Foundry, One Cyclotron Road, Berkeley, California 94720, USA



(Received 25 January 2020; accepted 26 March 2020; published 20 May 2020)

The synthesis of new materials with novel or useful properties is one of the most important drivers in the fields of condensed matter physics and materials science. Discoveries of this kind are especially significant when they point to promising future basic research and applications. van der Waals bonded materials comprised of lower-dimensional building blocks have been shown to exhibit emergent properties when isolated in an atomically thin form [1–8]. Here, we report the discovery of a transition metal chalcogenide in a heretofore unknown segmented linear chain form, where basic building blocks each consisting of two hafnium atoms and nine tellurium atoms ( $\text{Hf}_2\text{Te}_9$ ) are van der Waals bonded end to end. First-principle calculations based on density functional theory reveal striking crystal-symmetry-related features in the electronic structure of the segmented chain, including giant spin splitting and nontrivial topological phases of selected energy band states. Atomic-resolution scanning transmission electron microscopy reveals single segmented  $\text{Hf}_2\text{Te}_9$  chains isolated within the hollow cores of carbon nanotubes, with a structure consistent with theoretical predictions. van der Waals bonded segmented linear chain transition metal chalcogenide materials could open up new opportunities in low-dimensional, gate-tunable, magnetic, and topological crystalline systems.

DOI: 10.1103/PhysRevLett.124.206403

**Introduction.**—The isolation of single layers of van der Waals (vdW) bonded sheetlike materials has launched a new era of two-dimensional (2D) materials exploration, with the discovery of intriguing physical phenomena such as the fractional quantum Hall effect in graphene [1] and an indirect-to-direct band-gap transition for monolayers of the transition metal dichalcogenide  $\text{MoS}_2$  [2]. Recently, chain-like transition metal trichalcogenides have been examined at the one-dimensional (1D) limit inside carbon or boron nitride nanotubes, with, for example, charge-induced torsional waves appearing in single-chain  $\text{NbSe}_3$  [3].

Here, we investigate the transition metal chalcogenide (TMC) hafnium telluride (Hf-Te). Bulk  $\text{HfTe}_2$  is a semi-metal comprised of 2D layers with vdW bonds between layers [7,9], while bulk  $\text{HfTe}_3$  is a metal composed of 1D trigonal prismatic chains with vdW bonds between the chains [10,11]. Isolation of a monolayer of  $\text{HfTe}_2$  shows flattening of the valence band [7], while encapsulation of chains of  $\text{HfTe}_3$  within carbon nanotubes (CNTs) results in a size-driven metal-insulator transition as the chain number passes from 4 to 3 [4]. A single chain of  $\text{HfTe}_3$  encapsulated within a CNT supports a short-wavelength trigonal antiprismatic rocking distortion that drives a significant

energy gap, but the chain is otherwise structurally robust [4].

We show here that an entirely new low-dimensional form of Hf-Te is possible. The new form consists of structurally coherent zero-dimensional “blocks,” each comprised of two Hf atoms and nine Te atoms (i.e.,  $\text{Hf}_2\text{Te}_9$ ), arranged end to end in a *segmented linear chain*, with vdW bonds linking the blocks or chain segments. The segmented chain resides inside the hollow core of a CNT, which protects the chain from oxidation and facilitates experimental characterization. First-principles calculations reveal an especially rich electronic structure for the segmented chain. The bands near the chemical potential are fully spin polarized in one direction and  $k$ -dependent giant spin splitting of the bands occurs due to one mirror symmetry which is broken by crystal momentum  $k$  and another mirror symmetry which is preserved for all  $k$ . Calculated Zak phases of the bands suggest externally tunable topological invariance.

**Structural characterization.**—Segmented chain  $\text{Hf}_2\text{Te}_9$  specimens are synthesized using a method similar to that as described previously for the preparation of few-chain  $\text{HfTe}_3$  [4]. Briefly, end-opened multiwall carbon nanotubes are reacted together with Hf powder and Te shot, with

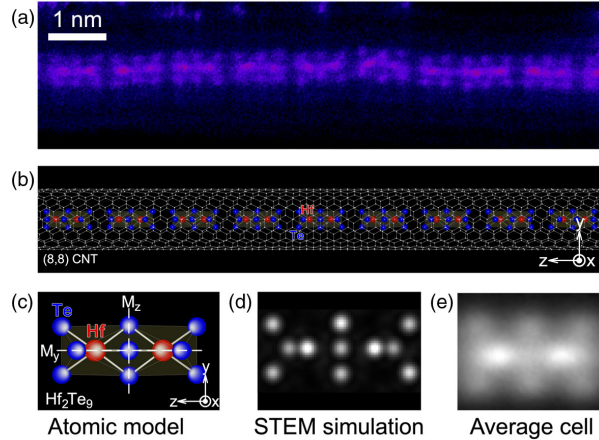


FIG. 1. The linear segmented chain of  $\text{Hf}_2\text{Te}_9$ . (a) Aberration-corrected HAADF STEM image of a segmented chain of  $\text{Hf}_2\text{Te}_9$  encapsulated within a double-walled CNT. A false color [Fire in the Look up Table (LUT) of ImageJ] is applied to visually aid the analysis. The structure consists of regularly spaced segments of  $\text{Hf}_2\text{Te}_9$  (or  $\text{Te}_3\text{-Hf-Te}_3\text{-Hf-Te}_3$ ). (b),(c) Atomic structure of the linear segmented chain of  $\text{Hf}_2\text{Te}_9$  obtained from DFT calculations. (b) The obtained atomic structure of the segmented chain inside an (8,8) single-wall CNT is shown, where Hf and Te atoms are represented as red and blue spheres, respectively, and the chain direction is set to the  $z$  direction. (c) The building block of a  $\text{Hf}_2\text{Te}_9$  unit is shown without a CNT for clearer presentation of the atomic structure, in which the mirror planes perpendicular to  $y$  and  $z$  axes are represented by white dashed lines and denoted as  $M_y$  and  $M_z$ , respectively. (d) Multislice simulated STEM image of a segment using the proposed atomic structure. (e) A composite STEM image generated from averaging experimentally collected 227 orientationally similar single segments (average cell).

iodine ( $\text{I}_2$ ) as a transport agent, in a sealed ampule at  $575^\circ\text{C}$  (see Supplemental Material [12] for details).

Figure 1 shows a structural characterization of a segmented  $\text{Hf}_2\text{Te}_9$  chain encapsulated within a CNT. Figure 1(a) shows an atomic-resolution high-angle annular dark-field (HAADF) scanning transmission electron microscopy (STEM) image of the chain. The inner diameter of the CNT host [not easily visible in Fig. 1(a)] is 1.1 nm. The chain is clearly and strikingly segmented into regularly spaced blocks, each with distinct substructure. Almost all (>95%) of the blocks imaged contain two bright spots in the center, suggestive of transition metal atoms, surrounded by a handful of dimmer spots, suggestive of chalcogen atoms.

To aid in the identification of the precise atomic structure of the blocks, we perform density functional theory (DFT) calculations. Several candidate structures of the segmented chain with various chemical formulas isolated in a vacuum region of  $50 \text{ \AA} \times 50 \text{ \AA}$  perpendicular to the chain are constructed, and the atomic positions of the candidate structures are fully relaxed by minimizing the total energy. Using the relaxed atomic positions of the segmented chain isolated in the vacuum and those of a pristine (8,8) CNT

(with inner diameter 1.1 nm), we construct the atomic structure of the segmented chain inside the (8,8) CNT. The atomic positions of the segmented chain are relaxed further by minimizing the total energy, while those of the CNT are fixed. The encapsulation does not alter the atomic structure of the segmented chain appreciably. Among all of the candidate structures investigated, only one relaxed structure, with a chemical formula of  $\text{Hf}_2\text{Te}_9$ , matches well with the experimental data.

Figures 1(b) and 1(c) show the theoretically predicted structure of the segmented chain encapsulated inside the (8,8) CNT. Figure 1(b) shows the segmented chain together with the CNT, while Fig. 1(c) shows the detailed structure of a single block (see Supplemental Material [12], Fig. S1, as well). The length of a block is  $7.89 \text{ \AA}$ , and blocks are separated by  $3.65 \text{ \AA}$ . The block atomic structure has two mirror symmetries, and the mirror planes perpendicular to the  $y$  and  $z$  axis are, respectively, denoted as  $M_y$  and  $M_z$  in Fig. 1(c). Each block has two Hf atoms and nine Te atoms, with the sequence  $\text{Te}_3\text{-Hf-Te}_3\text{-Hf-Te}_3$  along the chain ( $z$ ) direction. As shown additionally in Supplemental Material [12], Fig. S1, the adjacent three Te atoms form isosceles triangles. The isosceles triangle at the center of the block is on the mirror plane  $M_z$ , perpendicular to the chain direction, while those on the sides of the block cant toward the center of the block. Each Hf atom is surrounded by six Te atoms, forming a trigonal prismatic structure (Supplemental Material [12], Fig. S1), notably unlike the single-chain  $\text{HfTe}_3$ , which prefers a trigonal antiprismatic form [4]. (More details about the atomic structure models and symmetry are presented in Supplemental Material [12], Fig. S1.)

To further validate the proposed block atomic structure, we simulate a block STEM image, as shown in Fig. 1(d). To compare this prediction to experimental STEM data, we first generate a composite STEM image by averaging 227 orientationally similar experimental STEM single-block images, as shown in Fig. 1(e). Comparison of Figs. 1(d) and 1(e), as well as the dimensions of a block and the separation gap, shows good agreement between the theory and experiment. We have also performed electron energy loss spectroscopy (EELS) on segmented chain samples (see Supplemental Material [12]). The Te  $M$  edges of the EELS spectra are consistent with the atomic structure shown in Fig. 1(c). We note that previous studies have shown that CNTs can be filled by pure metals and pure chalcogens. We have performed control experiments and found no evidence for segmented chain structure within CNTs using only Hf, only Te, or only  $\text{I}_2$  as feedstock.

*Electronic structure.*—We investigate the electronic structure of the segmented  $\text{Hf}_2\text{Te}_9$  chain by DFT calculations. Because of the presence of the mirror symmetry with respect to the  $M_y$  plane [Fig. 1(c) and Supplemental Material [12], Fig. S1(b)], which is not broken by the crystal momentum  $k$ , the  $x$  and  $z$  components of spin and orbital angular momentum (OAM) with respect to the

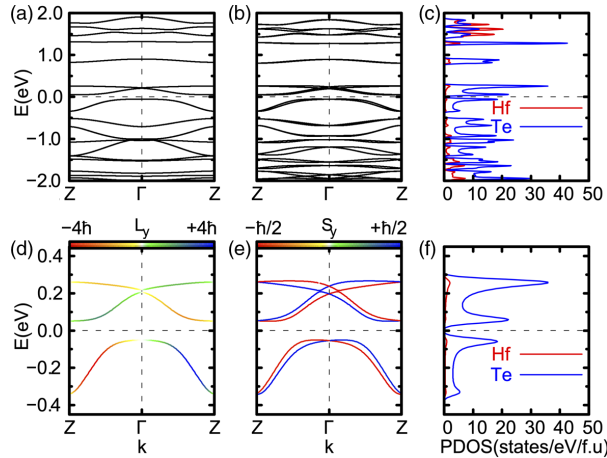


FIG. 2. Calculated electronic structures of the single-atomic segmented chain of  $\text{Hf}_2\text{Te}_9$ . (a)–(c) The electronic structure of an isolated segmented chain of  $\text{Hf}_2\text{Te}_9$ . The band structures obtained (a) without and (b) with considering SOI, and (c) PDOS obtained with SOI. (d)–(f) The electronic structure of the segmented chain  $\text{Hf}_2\text{Te}_9$  near the chemical potential. The band structures obtained (d) without and (e) with considering SOI, and (f) PDOS obtained with SOI. (d),(e) The color of the band lines represents the expectation value of the  $y$  component of OAM ( $L_y$ ) [in (d)] and spin ( $S_y$ ) [in (e)]. In (a)–(f), the chemical potential is set to zero and marked with a horizontal dashed line.

atomic positions on the plane should be zero regardless of  $k$  [21]. However, the crystal momentum  $k$  breaks the mirror symmetry with respect to the  $M_z$  plane, and the energy eigenstates are not the eigenstates of  $M_z$ , so the  $y$  component of the OAM of the states can have a finite value except for the time reversal invariant momentum points, the center, and the edge of the Brillouin zone ( $k = 0, \pi/a$ , where  $a$  is the unit cell length).

Figures 2(a) and 2(d) show the electronic band structure of the segmented chain isolated in a vacuum obtained without considering spin-orbit interaction (SOI). The bands in Fig. 2(d) are colored with the expectation values of the  $y$  component of the local OAM of the states  $|\psi_{nk}\rangle$ , with the band index  $n$  and the crystal momentum  $k$ , integrated over all the atoms in the unit cell,  $\langle L_y \rangle = \sum_{i \in \text{cell}} \langle L_y^i \rangle$ , where  $\langle L_y^i \rangle$  is the expectation value of the  $y$  component of the local OAM with respect to the  $i$ th atom of the states  $|\psi_{nk}\rangle$ . Figures 2(b) and 2(e) show the electronic band structure of the chain isolated in a vacuum obtained with considering SOI. The bands in Fig. 2(e) are colored with the expectation value of the  $y$  component of spin,  $\langle S_y \rangle$ , of the states. The unquenched  $L_y$  of the states near the chemical potential combined with the SOI causes a Rashba-type spin splitting of the bands proportional to  $L_y$ , resulting in fully spin-polarized states in the  $y$  direction. Because the states with opposite  $k$  have opposite spin polarization, directional currents can be generated using circularly polarized light as demonstrated through valley-photon coupling in 2D

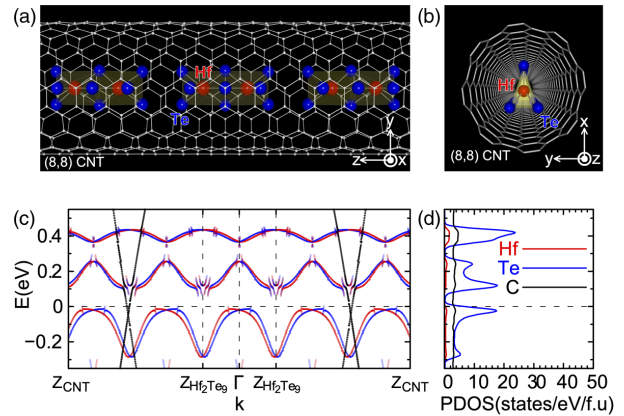


FIG. 3. Calculated atomic and electronic structures of a linear segmented chain of  $\text{Hf}_2\text{Te}_9$  encapsulated in an (8,8) CNT. (a),(b) Atomic structure of a segmented chain of  $\text{Hf}_2\text{Te}_9$  encapsulated within a CNT in (a) side view and (b) axial view, where Hf, Te, and C atoms are represented as red, blue, and white spheres, respectively. (c),(d) Electronic structure of the segmented chain  $\text{Hf}_2\text{Te}_9$  encapsulated in the CNT. (c) Band structure and (d) PDOS obtained with SOI. In (c),(d), the Fermi energy is set to zero and marked with a horizontal dashed line. In (c), band structures represented by red and blue dots are projected onto spin up and spin down, respectively, in the  $y$  direction of the segmented chain and unfolded with respect to the first Brillouin zone of the unit cell of the segmented chain, while the bands represented by black dots are projected onto the CNT and unfolded with respect to the first Brillouin zone of the unit cell of the CNT. The center of the Brillouin ( $k = 0$ ) is denoted by  $\Gamma$ , while  $Z_{\text{Hf}_2\text{Te}_9}$  and  $Z_{\text{CNT}}$  denote the zone boundaries for the segmented chain and the CNT, respectively.

transition metal dichalcogenides [22,23]. The calculated band gap is 100.3 meV, and the states near the chemical potential mostly derive from Te atoms, as shown in Figs. 2(c) and 2(f).

Figure 3 shows the calculated atomic and electronic structures of the segmented chain encapsulated inside an (8,8) CNT. The encapsulation does not alter the electronic structure of the segmented chain significantly except for the band repulsion at  $\sim 0.3$  eV above the Fermi energy. The states near the chemical potential remain fully spin polarized in the  $y$  direction, and the energy difference between the top of the highest occupied band and the bottom of the lowest unoccupied band remains at  $\sim 100$  meV, similar to that of the chain isolated in a vacuum. No appreciable covalent bonding between the chain and CNT is found. Mulliken charge analysis [24] reveals that the amount of charge transferred from the CNT to the segmented chain is  $0.118 e/\text{Hf}_2\text{Te}_9$  formula unit (f.u.), where  $e$  is the electron charge. The binding energy of the chain,  $E_b$ , is calculated to be 3.32 eV/f.u., which is defined as  $E_b = E_{\text{Hf}_2\text{Te}_9} + E_{\text{CNT}} - E_{\text{Hf}_2\text{Te}_9/\text{CNT}}$ , where  $E_{\text{Hf}_2\text{Te}_9}$ ,  $E_{\text{CNT}}$ , and  $E_{\text{Hf}_2\text{Te}_9/\text{CNT}}$  are the total energies of the segmented chain isolated in a vacuum, an empty CNT, and the

joint system of the chain encapsulated inside the CNT, respectively.

**Topological properties.**—We now consider the topological properties of the segmented chain. Because of the presence of time-reversal symmetry and mirror symmetry with respect to  $M_z$ , the Zak phase of the  $n$ th band,  $\gamma_n$ , is quantized to 0 or  $\pi$  (mod  $2\pi$ ) [25], corresponding to a topologically trivial or nontrivial band, respectively. The symmetry-protected topological invariance  $Z_2$  can be obtained by  $(-1)^{Z_2} = e^{i \sum_{n \in I} \gamma_n} = e^{2\pi i P^I / e}$ , where the sum of the Zak phase is over the occupied bands in only one channel  $\{u_{nk}^I\}$  out of two time-reversal channels  $\{u_{nk}^s\}$ ,  $s = I$  and  $II$ , and  $P^I$  is the partial polarization over channel I [26,27]. Since the sum of the Zak phase over one channel is nothing but the partial polarization of the channel, the  $Z_2$  invariance can be obtained alternatively by  $Z_2 = 2P^I / e = Q \bmod 2$ , where  $Q$  is the end charge of the finite-length chain [27,28].

We find that the topological invariance  $Z_2$  of the segmented chain can be tuned by doping as shown in Fig. 4. As shown in Figs. 4(a) and 4(b), in the neutral state  $Z_2 = 0$  for the infinite length  $\text{Hf}_2\text{Te}_9$  segmented chain, meaning the chain is a trivial insulator. We construct a finite length chain ( $\sim 15$  nm) and calculate the end charge  $Q$  (see Supplemental Material [12]); here  $Q = 0$ , confirming the topological triviality of the undoped material [27,28]. On the other hand, the highest occupied band is nontrivial and well separated from other bands as shown in Fig. 4(b). Therefore, if the system is hole doped ( $h$  doped) so that the chemical potential lies between the energy levels of the highest and the second-highest occupied band as illustrated in Figs. 4(c) and 4(d), it becomes a topological mirror insulator, provided that the Zak phases of the bands remain unchanged and that Hamiltonian of the  $h$ -doped system may be obtained adiabatically from the neutral chain without closing the band gap. That is, the number of nontrivial occupied bands in one channel changes from even to odd, and the sum of the Zak phase of the  $h$ -doped chain in one channel differs from that of a neutral chain by  $\pi$ , owing to the emptying out of the nontrivial highest occupied band. Hence, upon doping,  $Z_2$  changes from 0 to 1, meaning the segmented chain experiences a transition from a trivial insulator to a topological mirror insulator.

We verify this topological richness with an explicit calculation of  $Z_2$  invariance for an  $h$ -doped chain as shown in Figs. 4(c) and 4(d) (see Supplemental Material [12] as well). To simulate the hole-doped system, we subtract  $2e/f.u.$  from the neutral system in the DFT calculation. With the subtracted number of electrons, the topological invariance is  $Z_2 = 1$ , and the end charge of the finite length chain ( $\sim 15$  nm) is  $Q = 3e$ . Many studies for related systems have shown that the chemical potential can be readily altered by chemical doping [29–31], electrostatic gating [6,32,33], or application of pressure [34]. This suggests that the segmented chain  $\text{Hf}_2\text{Te}_9$  represents a

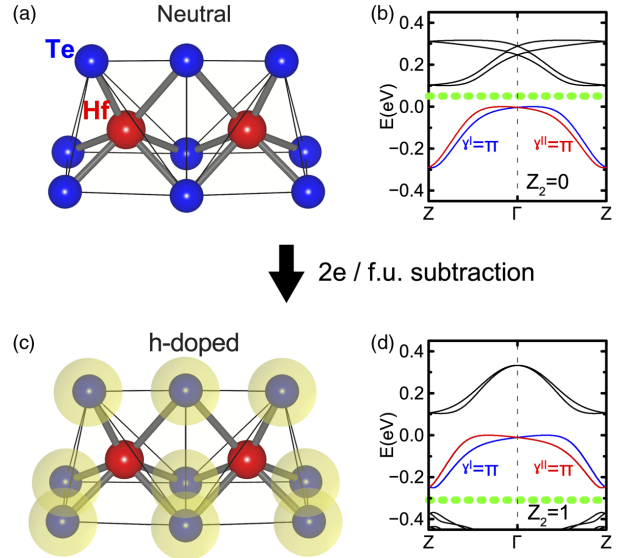


FIG. 4. Topological properties of a single-atomic segmented chain of  $\text{Hf}_2\text{Te}_9$  with various chemical potentials. (a),(b) The atomic and electronic structures of the segmented chain of  $\text{Hf}_2\text{Te}_9$  without a chemical potential change are shown for comparison. The highest occupied band is nontrivial. (c),(d) The atomic and electronic structure of the segmented chain of  $\text{Hf}_2\text{Te}_9$  with  $2e/f.u.$  subtracted in the DFT calculations. In (a), (c), Hf and Te atoms are represented as red and blue spheres, respectively. In (c), the subtracted charge is schematically represented by yellow spheres. In (b),(d), the energy level of the top of the highest occupied band is set to zero for easy comparison, and the chemical potential is represented by green dashed lines. Two time-reversal channels of the highest occupied bands,  $s = I$  and  $II$ , are represented by blue and red lines, respectively. The symmetry-protected topological invariance  $Z_2$  is 0 for a neutral system and 1 for the  $h$ -doped system.

versatile, highly unusual, and externally tunable topological material. We note that the  $\text{Hf}_2\text{Te}_9$  segmented chain is, to our knowledge, the first example of a vdW-bonded crystalline material with spatial-symmetry topological invariants [35,36]. Our discovery thus expands the class of realized topological states of matter.

**Conclusion.**—In conclusion, a TMC-based, vdW-bonded segmented linear chain  $\text{Hf}_2\text{Te}_9$  material has been synthesized within a protective CNT cage and its structure determined via STEM analysis and complementary DFT calculations. Theory also reveals giant spin splitting and crystal-symmetry-protected topological properties, which are promising for applications such as spintronic nano-devices and topological transistors. The segmented linear chain is a realization of a TMC in the quasi-0D limit, where 0D blocks are vdW end-to-end bonded in a linear chain. This quasi-0D material completes the family of dimensionally reduced TMCs, where bulk  $\text{MX}_2$  compounds are typically quasi-2D and  $\text{MX}_3$  compounds are typically quasi-1D ( $M =$  transition metal and  $X =$  chalcogen).

This work was primarily funded by the U.S. Department of Energy, Office of Science, Office of Basic Energy Sciences, Materials Sciences and Engineering Division, under Contract No. DE-AC02-05-CH11231 within the sp<sup>2</sup>-Bonded Materials Program (KC2207) which provided for synthesis of the chains, TEM structural characterization, and theoretical modeling of relaxed structure of one segment Hf<sub>2</sub>Te<sub>9</sub>. The elemental mapping work was funded by the U.S. Department of Energy, Office of Science, Office of Basic Energy Sciences, Materials Sciences and Engineering Division, under Contract No. DE-AC02-05-CH11231 within the van der Waals Heterostructures Program (KCWF16). Work at the Molecular Foundry (TEAM 0.5 characterization) was supported by the Office of Science, Office of Basic Energy Sciences, of the U.S. Department of Energy under Contract No. DE-AC02-05-CH11231. Support was also provided by the National Science Foundation under Grants No. DMR-1807233, which provided for preparation of opened nanotubes, and No. DMR-1926004, which provided for theoretical calculations of the electronic band structure of the segmented chain. Computational resources were provided by the DOE at Lawrence Berkeley National Laboratory's NERSC facility and the NSF through XSEDE resources at NICS.

The authors declare no competing interests.

T. P., S. O., M. L. C., and A. Z. conceived the idea. S. S. synthesized materials. T. P., S. S., B. S., J. D. C., C. S., and P. E. performed electron microscopy, data acquisition, and analysis. S. O. carried out density functional calculations. S. O. and M. L. C. did the theoretical analysis. M. L. C. and A. Z. supervised the project. T. P., S. O., S. S., M. L. C., and A. Z. wrote the manuscript with contribution from all other authors.

\*These authors contributed equally to this work.

†To whom all correspondence should be addressed.  
azettl@berkeley.edu

- [1] K. I. Bolotin, F. Ghahari, M. D. Shulman, H. L. Stormer, and P. Kim, *Nature (London)* **462**, 196 (2009).
- [2] K. F. Mak, C. Lee, J. Hone, J. Shan, and T. F. Heinz, *Phys. Rev. Lett.* **105**, 136805 (2010).
- [3] T. Pham, S. Oh, P. Stetz, S. Onishi, C. Kisielowski, M. L. Cohen, and A. Zettl, *Science* **361**, 263 (2018).
- [4] S. Meyer, T. Pham, S. Oh, P. Ercius, C. Kisielowski, M. L. Cohen, and A. Zettl, *Phys. Rev. B* **100**, 041403(R) (2019).
- [5] K. S. Novoselov, D. Jiang, F. Schedin, T. J. Booth, V. V. Khotkevich, S. V. Morozov, and A. K. Geim, *Proc. Natl. Acad. Sci. U.S.A.* **102**, 10451 (2005).
- [6] K. S. Novoselov, A. K. Geim, S. V. Morozov, D. Jiang, Y. Zhang, S. V. Dubonos, I. V. Grigorieva, and A. A. Firsov, *Science* **306**, 666 (2004).
- [7] Y. Nakata, K. Sugawara, A. Chainani, K. Yamauchi, K. Nakayama, S. Souma, P. Y. Chuang, C. M. Cheng, T. Oguchi, K. Ueno, T. Takahashi, and T. Sato, *Phys. Rev. Mater.* **3**, 071001 (2019).
- [8] M. Nagata, S. Shukla, Y. Nakanishi, Z. Liu, Y.-C. Lin, T. Shiga, Y. Nakamura, T. Koyama, H. Kishida, T. Inoue, N. Kanda, S. Ohno, Y. Sakagawa, K. Suenaga, and H. Shinohara, *Nano Lett.* **19**, 4845 (2019).
- [9] S. Aminalragia-Giamini, J. Marquez-Velasco, P. Tsipas, D. Tsoutsou, G. Renaud, and A. Dimoulas, *2D Mater.* **4**, 015001 (2017).
- [10] J. Li, J. Peng, S. Zhang, and G. Chen, *Phys. Rev. B* **96**, 174510 (2017).
- [11] S. J. Denholme, A. Yukawa, K. Tsumura, M. Nagao, R. Tamura, S. Watauchi, I. Tanaka, H. Takayanagi, and N. Miyakawa, *Sci. Rep.* **7**, 45217 (2017).
- [12] See Supplemental Material at <http://link.aps.org/supplemental/10.1103/PhysRevLett.124.206403> for details of materials synthesis, materials characterization, and calculation methods, which includes Refs. [13–20].
- [13] J. P. Perdew, K. Burke, and M. Ernzerhof, *Phys. Rev. Lett.* **77**, 3865 (1996).
- [14] N. Troullier and J. L. Martins, *Phys. Rev. B* **43**, 1993 (1991).
- [15] J. M. Soler, E. Artacho, J. D. Gale, A. García, J. Junquera, P. Ordejón, and D. Sánchez-Portal, *J. Phys. Condens. Matter* **14**, 2745 (2002).
- [16] L. Kleinman, *Phys. Rev. B* **21**, 2630 (1980).
- [17] G. Theurich and N. A. Hill, *Phys. Rev. B* **64**, 073106 (2001).
- [18] L. Kleinman and D. M. Bylander, *Phys. Rev. Lett.* **48**, 1425 (1982).
- [19] S. Grimme, *J. Comput. Chem.* **27**, 1787 (2006).
- [20] M. L. Cohen, M. Schlüter, J. R. Chelikowsky, and S. G. Louie, *Phys. Rev. B* **12**, 5575 (1975).
- [21] S. Oh and H. J. Choi, *Sci. Rep.* **7**, 2024 (2017).
- [22] S. H. Gong, F. Alpeggiani, B. Sciacca, E. C. Garnett, and L. Kuipers, *Science* **359**, 443 (2018).
- [23] C. Jin, J. Kim, M. Iqbal Bakti Utama, E. C. Regan, H. Kleemann, H. Cai, Y. Shen, M. J. Shinner, A. Sengupta, K. Watanabe, T. Taniguchi, S. Tongay, A. Zettl, and F. Wang, *Science* **360**, 893 (2018).
- [24] R. S. Mulliken, *J. Chem. Phys.* **23**, 1833 (1955).
- [25] J. Zak, *Phys. Rev. Lett.* **62**, 2747 (1989).
- [26] L. Fu and C. L. Kane, *Phys. Rev. B* **76**, 045302 (2007).
- [27] A. Lau, J. van den Brink, and C. Ortix, *Phys. Rev. B* **94**, 165164 (2016).
- [28] G. Van Miert and C. Ortix, *Phys. Rev. B* **96**, 235130 (2017).
- [29] H. S. Lee, S. Park, J. Y. Lim, S. Yu, J. Ahn, D. K. Hwang, Y. Sim, J. Lee, M. Seong, S. Oh, H. J. Choi, and S. Im, *Small* **15**, 1901793 (2019).
- [30] S. Oh, J. Y. Lim, S. Im, and H. J. Choi, *Phys. Rev. B* **100**, 085416 (2019).
- [31] T. Cao, F. Zhao, and S. G. Louie, *Phys. Rev. Lett.* **119**, 076401 (2017).
- [32] S. Oh, M. F. Crommie, and M. L. Cohen, *ACS Nano* **13**, 1713 (2019).
- [33] K. S. Novoselov, A. K. Geim, S. V. Morozov, D. Jiang, M. I. Katsnelson, I. V. Grigorieva, S. V. Dubonos, and A. A. Firsov, *Nature (London)* **438**, 197 (2005).
- [34] B. Yang, F. Liu, and M. G. Lagally, *Phys. Rev. Lett.* **92**, 025502 (2004).
- [35] L. Fu, *Phys. Rev. Lett.* **106**, 106802 (2011).
- [36] Y. Ando and L. Fu, *Annu. Rev. Condens. Matter Phys.* **6**, 361 (2015).